Anal. Chem. **2004,** *76,* 1089−1097

Characterization of Carbon/Nitroazobenzene/Titanium Molecular Electronic Junctions with Photoelectron and Raman Spectroscopy

Aletha M. Nowak and Richard L. McCreery*

Department of Chemistry, The Ohio State University, 100 West 18th Avenue, Columbus, Ohio 43210-1185

Molecular junctions consisting of nitroazobenzene (NAB) chemisorbed to a substrate of pyrolyzed photoresist film (PPF) and a top contact of vapor-deposited titanium were examined with Raman spectroscopy and X-ray photoelectron spectroscopy (XPS). The thickness of the NAB layer varied from submonolayer to 4.5 nm, and a thin (1−3 nm) overlayer of Ti was deposited by electron beam deposition. Without Ti, the NAB surface Raman spectrum was sufficiently strong to observe previously unreported modes in the 500−1000-cm^{-1} region, and the 1000−1700-cm^{-1} region was sufficiently strong to observe the effects of metal deposition. Upon Ti deposition, the intensities of NAB modes associated with the nitro group decreased significantly, and the XPS indicated formation of a Ti−N bond. For the thicker NAB layers (1.9 and 4.5 nm), the intensities of the NO_2 Raman modes partially recovered over a several-day period, but they remain depressed or absent in the submonolayer sample. The results indicate a reaction between condensing Ti atoms and the terminal NO_2 group, probably to form a Ti−nitroso linkage between NAB and Ti. The result is a molecular junction with covalent bonding at both ends in the form of a C−C bond between PPF and NAB and a Ti−N bond to the top contact. The structural implications of the current results are interpreted in the context of recently reported functioning PPF/NAB/Ti molecular electronic junctions. In particular, the reaction between Ti and the nitro group appears to prevent short circuits resulting from incursion of Ti into the NAB layer.

Much of the allure of molecular electronics lies in the possibility of incorporating molecules into electronic circuits, thereby fabricating microelectronic devices with diverse electronic properties. Of particular relevance here are molecular junctions composed of an array of molecules or a single molecule between two conventional conductors. An extensive effort has been expended to determine a variety of current−voltage responses of molecular junctions, such as rectification,[1−4] negative differential resistance,[5] conductance switching,[1,6−9] photocurrent,[10−13] and various electron transport mechanisms.[3−5,14−18] To date, the majority of this research has been performed on self-assembled organothiolate monolayers on gold substrates (SAMs)[4,5,16,19−21] or Langmuir−Blodgett (L−B)[2,3,7] films with either vapor-deposited metals, a mercury drop, or a scanning probe microscopy tip to complete the circuit. While these systems have exhibited interesting electronic behavior, they are difficult to characterize structurally with conventional spectroscopic techniques. Little is known about molecular structure once a molecule is part of a circuit, since the materials used for the contacts are generally not transparent to visible or infrared radiation, and are not amenable to NMR or mass spectrometry. Thus far, structural information is generally limited to examining the junction without a top contact [2,3] or performing X-ray photoelectron spectroscopy (XPS) through a very thin metal over-layer.[22−30]

* Corresponding author. Phone: 614-292-2021. E-mail: mccreery.2@osu.edu.

(1) McCreery, R. L.; Dieringer, J.; Solak, A. O.; Snyder, B.; Nowak, A.; McGovern, W. R.; DuVall, S. *J. Am. Chem. Soc.* **2003**, *125*, 10748.
(2) Metzger, R. M.; Chen, B.; Hopfner, U.; Lakshmikantham, M. V.; Vuillaume, D.; Kawai, T.; Wu, X.; Tachibana, H.; Hughes, T. V.; Sakurai, H.; Baldwin, J. W.; Hosch, C.; Cava, M. P.; Brehmer, L.; Ashwell, G. J. *J. Am. Chem. Soc.* **1997**, *119*, 10455.
(3) Metzger, R. M.; Xu, T.; Peterson, I. R. *J. Phys. Chem. B* **2001**, *105*, 7280.
(4) Zhou, C.; Deshpande, M. R.; Reed, M. A.; Jones, L.; Tour, J. M. *Appl. Phys. Lett.* **1997**, *71*, 611.
(5) Chen, J.; Reed, M. A.; Rawlett, A. M.; Tour, J. M. *Science* **1999**, *286*.
(6) Ranganathan, S.; Steidel, I.; Anariba, F.; McCreery, R. L. *Nano Lett.* **2001**, *1*, 491.
(7) Collier, C. P.; Wong, E. W.; Belohradsky, M.; Raymo, F. M.; Stoddart, J. F.; Kuekes, P. J.; Williams, R. S.; Heath, J. R. *Science* **1999**, *285*, 391.
(8) Donhauser, Z. J.; Mantooth, B. A.; Kelly, K. F.; Bumm, L. A.; Monnell, J. D.; Stapleton, J. J.; Price, D. W.; Rawlett, A. M.; Allara, D. L.; Tour, J. M.; Weiss, P. S. *Science* **2001**, *292*, 2303.
(9) Ramachandran, G. K.; Hopson, T. J.; Rawlett, A. M.; Nagahara, L. A.; Primak, A.; Lindsay, S. M. *Science* **2003**, *300*, 1413.
(10) Velez, M.; Mukhopadhyay, S.; Muzikante, I.; Matisova, G.; Vieira, S. *Langmuir* **1997**, *13*, 870.
(11) Delaire, J. A.; Nakatani, K. *Chem. Rev.* **2000**, *100*, 1817.
(12) Matsumoto, M.; Terrettaz, S.; Tachibana, H. *Adv. Colloid Interface Sci.* **2000**, *87*, 147.
(13) Matisova, G.; Markava, E.; Muzikante, I.; Fonavs, E.; Gerca, L. *Adv. Mater. Opt. Electron.* **1996**, *6*, 279.
(14) Anariba, F.; McCreery, R. L. *J. Phys. Chem. B* **2002**, *106*, 10355.
(15) Hong, S.; Reifenberger, R.; Tian, W.; Datta, S.; Henderson, J.; Kubiak, C. P. *Superlattices Microstruct.* **2000**, *28*, 289.
(16) Rampi, M. A.; Whitesides, G. M. *Chem. Phys.* **2002**, *281*, 373.
(17) Mujica, V.; Ratner, M. A. *Chem. Phys.* **2001**, *264*, 365.
(18) Mujica, V.; Roitberg, A. E.; Ratner, M. A. *J. Phys. Chem.* **2000**, *112*, 6834.
(19) Chen, J.; Calvet, L. C.; Reed, M. A.; Carr, D. W.; Grubisha, D. S.; Bennett, D. W. *Chem. Phys. Lett.* **1999**, *313*, 741.
(20) Holmlin, R. E.; Haag, R.; Chabinyc, M. L.; Ismagilov, R. F.; Cohen, A. E.; Terfort, A.; Rampi, M. A.; Whitesides, G. M. *J. Am. Chem. Soc.* **2001**, *123*, 5075.
(21) Slowinski, K.; Majda, M. *J. Electrol. Chem.* **2000**, *491*, 139.
(22) Konstadinidis, K.; Zhang, P.; Opila, R. L.; Allara, D. L. *Surf. Sci.* **1995**, *338*, 300.
(23) Jung, D. R.; Czanderna, A. W.; Herdt, G. C. *J. Vac. Sci. Technol. A* **1996**, *14*, 1779.

10.1021/ac034807w CCC: $27.50
Published on Web 01/09/2004

In recent reports, we described an alternative approach to molecular junction fabrication, which yields reproducible molecular junctions exhibiting rectification and conductance switching.[1,6,31] Junction assembly begins with a covalently bound mono- or multilayer of the molecule of interest on a flat graphitic carbon substrate. A variety of molecules, including nitroazobenzene (NAB), biphenyl, nitrobiphenyl, etc., may be bonded to the substrate by electrochemical reduction of the corresponding diazonium ion. Multilayer formation may occur under certain conditions via radical attachment to the surface-bound layer forming carbon−carbon bonds between phenyl rings.[32] Molecular monolayers on carbon substrates prepared via diazonium reduction have been characterized extensively, with XPS, Raman and FT-IR spectroscopy, STM, AFM, and related techniques.[32−40]

Application of the top contact to SAM and L−B monolayers has proven to be a challenging problem due to the likelihood of disturbing the molecular layer during metal condensation. For example, evaporated Ag and Au atoms penetrated an alkanethiol SAM, resulting in the "top" contact ending up underneath the original monolayer.[28−30] Our approach here uses titanium as the top contact, based partly on reported success fabricating metal/SAM/Ti junctions.[4,41,42] Titanium was deposited by e-beam evaporation through a shadow mask, followed by a layer of Au without breaking the vacuum. Titanium is considered a reactive metal, due to its reduction potential ($E° = -1.6$ V vs NHE), its high free energy in the vapor phase, and its ability to form bonds with oxygen, carbon, and nitrogen. The relationship between functional group reactivity and penetration of vapor-deposited Ti into a Au/thiol SAM has been examined by XPS and infrared spectroscopy.[22,23] The results indicate that reactive functional groups containing oxygen and nitrogen prevent the intrusion of Ti atoms into the monolayer. Similar results were found while studying the chemical interaction between Ti and functional groups in polymer films,[43−45] in which often only the surface functional groups react with titanium.[45]

In the current report, Raman spectroscopy and XPS were used to probe the interaction between vapor-deposited Ti and a nitroazobenzene-modified carbon substrate. Critical objectives of the investigation were examining the structural integrity of the NAB mono- or multilayer upon Ti deposition and revealing the nature of the Ti/NAB interaction. We chose NAB as an initial molecule for study due to its relatively strong Raman scattering and previous characterization of NAB monolayers on carbon surfaces. In the current work, a very thin (1−3 nm) layer of Ti was deposited on NAB mono- and multilayers, to achieve optical transparency. The thin Ti layer permitted characterization of the NAB layer as it is expected to exist in a functional molecular junction. A variety of NAB thicknesses was studied, including a spontaneously adsorbed submonolayer, near-monolayer (1.9 nm), and a relatively thick (4.5 nm) film.

EXPERIMENTAL SECTION

Pyrolyzed photoresist films (PPF) were prepared using established procedures,[46,47] on 1 × 1 cm pieces of silicon (p-type, boron doped, 1 Ω cm^2, 2 mm thick), which were sonicated in acetone (Mallinckrodt AR, 99.7%) for 45 min and dried with argon. The clean silicon pieces were spin coated at 6000 rpm for 30 s with positive photoresist AZ P4330-RS (Clariant Corp.). Several applications were applied to yield a total thickness of 5−7 μm. Samples were soft baked at 90 °C for 20 min before pyrolysis. Pyrolysis took place in a tube furnace (Lindberg Blue) fitted with a 1-in.-diameter quartz tube. Samples were heated at 8 °C/min to 1000 °C and then held for 1 h in the presence of forming gas (95% nitrogen and 5% hydrogen) flowing at 100 mL/min throughout the pyrolysis procedure. Prior to surface derivatization, samples were cleaned in acetonitrile (Sigma-Aldrich, 99.5+%), which had been purified with activated carbon and then filtered using 0.2-μm filters (Millipore).[48]

Because film thickness is strongly dependent upon derivatization potential, the Ag^+/Ag reference electrode (0.01 M $AgNO_3$ and 0.1 M tetrabutylammonium tetrafluoroborate (TBATFB, Aldrich, 99%) in acetonitrile) was checked for potential drift before use. The reference electrode was calibrated against the $E_{1/2}$ for the oxidation of ferrocene (0.3 mM ferrocene (Sigma) and 0.1 M TBATFB in acetonitrile). The measured ferrocene $E_{1/2}$ was 93.4 (±3.3) mV on a Pt electrode at 200 mV/s, yielding a Ag^+/Ag potential of 214 mV versus aqueous SCE.

4-Nitroazobenzene 4′-diazonium tetrafluoroborate salts were prepared as previously described.[37,40,49,50] Electrochemical derivatization was preformed using an acetonitrile solution containing 1 mM diazonium salt and 0.1 M TBATFB as the supporting electrolyte. The solution was purged with argon for 20 min before derivatization. Deposition conditions were chosen such that

(24) Herdt, G. C.; Jung, D. R.; Czanderna, A. W. *J. Adhes.* **1997**, *60*, 197.
(25) Herdt, G. C.; Czanderna, A. W. *J. Vac. Sci. Technol. A* **1999**, *17*, 3415.
(26) Dake, L. S.; King, D. E.; Czanderna, A. W. *Solid State Sci.* **2000**, *2*, 781.
(27) Hooper, A.; Fisher, G. L.; Konstadinidis, K.; Jung, D.; Nguyen, H.; Opila, R.; Collins, R. W.; Winograd, N.; Allara, D. L. *J. Am. Chem. Soc.* **1999**, *121*, 8052.
(28) Fisher, G. L.; Hooper, A.; Opila, R. L.; Jung, D. R.; Allara, D. L.; Winograd, N. *J. Electron Spectrosc. Relat. Phenom.* **1999**, *98−99*, 139.
(29) Fisher, G. L.; Hooper, A. E.; Opila, R. L.; Jung, D. R.; Allara, D. L.; Winograd, N. *J. Phys. Chem. B* **2000**, *104*, 3267.
(30) Fisher, G. L.; Walker, A. V.; Hooper, A. E.; Tighe, T. B.; Bahnck, K. B.; Skriba, H. T.; Reinard, M. D.; Haynie, B. C.; Opila, R. L.; Winograd, N.; Allara, D. L. *J. Am. Chem. Soc.* **2002**, *124*, 5528.
(31) Solak, A. O.; Ranganathan, S.; Itoh, T.; McCreery, R. L. *Electrochem. Solid State Lett.* **2002**, *5*, E43.
(32) Kariuki, J. K.; McDermott, M. T. *Langmuir* **2001**, *17*, 5947.
(33) Liu, Y.-C.; McCreery, R. L. *Anal. Chem.* **1997**, *69*, 2091.
(34) Liu, Y.-C.; McCreery, R. L. *J. Am. Chem. Soc.* **1995**, *117*, 11254.
(35) Anariba, F.; DuVall, S. H.; McCreery, R. L. *Anal. Chem.* **2003**, *75*, 3837.
(36) Itoh, T.; McCreery, R. L. *J. Am. Chem. Soc.* **2002**, *124*, 10894.
(37) Allongue, P.; Delamar, M.; Desbat, B.; Fagebaume, O.; Hitmi, R.; Pinson, J.; Saveant, J. M. *J. Am. Chem. Soc.* **1997**, *119*, 201.
(38) Coulon, E.; Pinson, J.; Bourzat, J.-D.; Commercon, A.; Pulicani, J.-P. *Langmuir* **2002**, *17*, 7102.
(39) Delamar, M.; Desarmot, G.; Fagebaume, O.; Hitmi, R.; Pinson, J.; Saveant, J. *Carbon* **1997**, *35*, 801.
(40) Delamar, M.; Hitmi, R.; Pinson, J.; Saveant, J. M. *J. Am. Chem. Soc.* **1992**, *114*, 5883.
(41) Reed, M. A.; Zhou, C.; Muller, C. J.; Burgin, T. P.; Tour, J. M. *Science* **1997**, *278*, 252.
(42) Chen, J.; Wang, W.; Reed, M. A.; Rawlett, A. M.; Price, D. W.; Tour, J. M. *Appl. Phys. Lett.* **2000**, *77*, 1224.
(43) Konstadinidis, K.; Opila, D. R.; Taylor, J. A.; Miller, A. C. *J. Adhes.* **1994**, *46*, 197.
(44) Ohuchi, F. S.; Freilich, S. C. *J. Vac. Sci. Technol. A* **1986**, *4*, 1039.
(45) Bou, M.; Martin, J. M.; Mogne, T. L. *Appl. Surf. Sci.* **1991**, *47*, 149.
(46) Ranganathan, S.; McCreery, R. L. *Anal. Chem.* **2001**, *73*, 893.
(47) Ranganathan, S.; McCreery, R. L.; Majji, S. M.; Madou, M. *J. Electrochem. Soc.* **2000**, *147*, 277.
(48) Ranganathan, S.; Kuo, T.-C.; McCreery, R. L. *Anal. Chem.* **1999**, *71*, 3574.
(49) Yang, H.-H.; McCreery, R. L. *J. Electrochem. Soc.* **2000**, *147*, 3420.
(50) DuVall, S.; McCreery, R. L. *J. Am. Chem. Soc.* **2000**, *122*, 6759.

samples of various NAB thicknesses were prepared. The applied potential was scanned at 200 mV/s for either one cycle from + 400 to −200 mV or four cycles from +400 to −600 mV versus Ag/Ag^+. These conditions produced NAB layers covalently bonded to the PPF, which were 1.88 ± 0.14 and 4.51 ± 0.7 nm thick, respectively. An atomic force microscopy (AFM) scratching technique described elsewhere was used to measure NAB thickness.[35] It involves making a deliberate scratch in the modified layer using contact mode AFM and then measuring the depth of the scratch with tapping mode AFM. Samples of chemisorbed NAB on PPF will be referred to as NAB(1.9)/PPF and NAB(4.5)/PPF, depending on thickness.

NAB samples of submonolayer thickness were prepared by the spontaneous reduction and chemisorption of the corresponding diazonium reagent.[36] PPF samples were submerged in the derivatization solution for 15 min at open circuit. All NAB-modified samples were rinsed with the filtered acetonitrile and dried in argon. The surface coverage of the submonolayer was estimated from the N_{1s} and C_{1s} XPS peak areas,[51] by comparison to the NAB-(1.9) spectrum. The N/C ratio of 0.082 for the NAB(1.9)/PPF sample yields a surface coverage of $(2-4) \times 10^{-10}$ mol/cm^2, close to the expected value for a monolayer. The 0.027 N/C ratio observed for the submonolayer sample corresponds to ~32% of a monolayer. The submonolayer sample has an apparent average thickness of 0.6 nm and will be referred to as NAB(0.6)/PPF. Immediately after derivatization, samples were loaded into an electron beam evaporator (Veeco/Telemark), which was described elsewhere.[1] Approximately 1.0 or 3.0 nm of Au or Ti was deposited on half of the sample at a deposition rate of 0.03 nm/s, while a contact mask covered the remaining half. Metal deposition was monitored in situ by a quartz crystal microbalance. The base pressure of the deposition chamber was less than 8×10^{-6} Torr during metal deposition. To promote even metal deposition, samples were rotated at ~1 revolution/s. No noticeable effects were observed in the Raman spectra collected from samples prepared with lower base pressure (5×10^{-7} Torr). The transparency of a 1.0-nm Ti layer deposited on quartz was determined with a UV−visible spectrometer (Perkin-Elmer, Lambda 900). For the wavelength range from 500 to 800 nm, the observed transmission was 94% versus a quartz background.

Raman spectra were collected with a line-focused $f/2$ Raman spectrometer (Chromex) and a back-thinned CCD (Andor), described previously.[52] A 514.5-nm argon ion laser (Coherent) with a power of 45 mW at the sample was used, unless noted otherwise. The focal line was approximately 5 mm × 50 μm, and integration time for Raman spectrum acquisition was 30 s. Spectra were taken immediately after removing samples from the electron beam evaporator and at several times up to 2 weeks after metal deposition. Spectra presented in figures are averages of 10 integrations, and no spike removal procedures were employed. The Raman shift axis was calibrated with benzonitrile, and intensities were not corrected for instrument response. Peak center frequencies were determined with the "center X" peak marking function of Grams AI, version 6.00 (Galactic Industries, Salem, NH) or using the "curve fit" function where appropriate (mixed Gaussian−Lorentzian line shape, less than 50 iterations to achieve lowest χ^2).

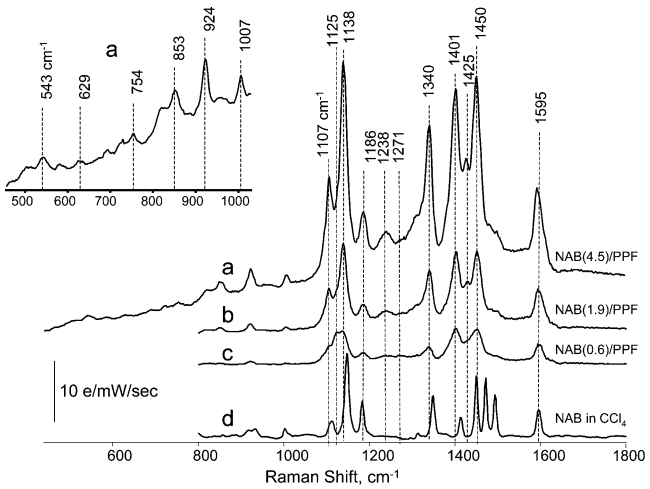

Figure 1. Raman spectra of nitroazobenzene layers on PPF, with NAB thicknesses of 4.5 (spectrum a) and 1.9 nm (b), plus a submonolayer with average thickness of 0.6 nm (c). Inset shows spectrum a in low-frequency region, with vertical scale expanded 10×. Surface spectra are averages of 10 acquisitions lasting 30 s each, with a laser power of 45 mW (514.5 nm) focused on a 0.05 × 5 mm line. The PPF substrate spectrum was mathematically subtracted. Spectrum d is NAB dissolved in CCl_4. Indicated peak frequencies should be considered labels, and specific peak frequencies are listed in Table 1. The intensity scale only applies to the spectra of NAB on PPF (a−c).

The XPS analysis was performed with a Kratos Axis Ultra spectrometer equipped with a monochromated Al Kα X-ray source. The base pressure of the analysis chamber was less than 1×10^{-9} Torr. A pass energy of 20 eV and step energy of 0.1 eV were used for all acquisitions. Peak fitting and integration were performed using the software provided with the instrument. Molecular modeling was performed with Gaussian 98[53] using the density functional method B3LYP with the 6-31G(d) basis set on a Linux-based workstation (Dell, Precision 420 WorkStation).

RESULTS

Raman Spectroscopy. Chemisorbed NAB was used in this study due to its large Raman cross section,[33,36] its application in molecular junctions,[6,31] and ability to form layers of variable thickness.[35] Raman spectra were obtained on samples of varying NAB thickness from both the sample region exposed to titanium and the region protected by the mask. The spectra for submonolayer, 1.9- and 4.5-nm-thick NAB/PPF without titanium are shown in Figure 1, along with a spectrum of NAB in CCl_4 solution. The spectrum collected from submonolayer NAB (Figure 1c) is very

(51) Kuo, T.-C.; McCreery, R. L.; Swain, G. M. *Electrochem. Solid State Lett.* **1999**, *2*, 288.

(52) Ramsey, J. D.; Ranganathan, S.; Zhao, J.; McCreery, R. L. *Appl. Spectrosc.* **2001**, *55*, 767.

(53) Frisch, M. J.; Trucks, G. W.; Schlegel, H. B.; Scuseria, G. E.; Robb, M. A.; Cheeseman, J. R.; Zakrzewski, V. G.; Montgomery, J. A., Jr.; Stratmann, R. E.; Burant, J. C.; Dapprich, S.; Millam, J. M.; Daniels, A. D.; Kudin, K. N.; Strain, M. C.; Farkas, O.; Tomasi, J.; Barone, V.; Cossi, M.; Cammi, R.; Mennucci, B.; Pomelli, C.; Adamo, C.; Clifford, S.; Ochterski, J.; Petersson, G. A.; Ayala, P. Y.; Cui, Q.; Morokuma, K.; Malick, D. K.; Rabuck, A. D.; Raghavachari, K.; Foresman, J. B.; Cioslowski, J.; Ortiz, J. V.; Stefanov, B. B.; Liu, G.; Liashenko, A.; Piskorz, P.; Komaromi, I.; Gomperts, R.; Martin, R. L.; Fox, D. J.; Keith, T.; Al-Laham, M. A.; Peng, C. Y.; Nanayakkara, A.; Gonzalez, C.; Challacombe, M.; Gill, P. M. W.; Johnson, B. G.; Chen, W.; Wong, M. W.; Andres, J. L.; Head-Gordon, M.; Replogle, E. S.; Pople, J. A. *Gaussian 98*, revision A.7; Gaussian, Inc.: Pittsburgh, PA, 1998.

Table 1. Raman Peak Frequencies and Assignments for Nitroazobenzene on PPF

free NAB in CCl_4	NAB(0.6) PPF[a]	NAB(1.9) PPF[a]	NAB(4.5) PPF[a]	calcd for 4-phenyl-NAB[b]	assgnmnt[c]	Umapathy calcd for 4-NAB[b,d]	assgnmnt and potential energy distributn[d,e](%)
525		544 (± 0.8)	543 (± 1.3)	536 (25)	uncertain	557 (56)	51 δ(C−N), 33 δ(C−C)
632		629 (± 1.4)[f]	629 (± 2.9)	613 (29)	ring deformation	646 (53)	94 δ(C−C)
770		754 (± 1.0)	754 (± 0.1)	723 (35)	ring deformation and NO_2 scissoring	716 (49)	73 δ(C−C), 12 δ(C−N)
858	855 (± 0.2)[g]	855 (± 1.2)	853 (± 0.6)	804 (38)	NO_2 bend		
933	924 (± 1.3)	923 (± 0.2)	924 (± 0.3)	934 (46)	CH bend	940 (41)	38 ν(C−C), 33 δ(C−C), 13 ν(C−N), 11 δ(N=N)
1002	1003 (± 1.2)	1007 (± 0.8)	1007 (± 0.4)	983 (54)	ring deformation	1039 (37)	73 δ(C−C), 22 ν(C−C)
1112		1106 (± 0.4)	1108 (± 0.4)	1086 (59)	phenyl−NO_2 stretch and C−H wag	1141 (31)	38 ν(C−C), 34 δ(C−C), 16 $\nu(C-N)_{NO}$
	1124 (± 0.9)						
1147	1137 (± 0.9)	1139 (± 0.1)	1140 (± 0.4)	1127 (62)	phenyl−NN stretch	1181 (29)	34 ν(C−N), 31 δ(C−C), 19 ν(C−C), 10 δ(C−N)
1183	1186 (± 0.7)	1185 (± 0.6)	1187 (± 0.5)	1172 (65)	CH bend	1226 (27)	48 ν(C−C), 48 δ(C−H)
	1238 (± 2.0)	1237 (± 1.0)	1240 (± 0.9)	1247 (68)	phenyl−NAB stretch		
	1271 (± 0.9)						
1347	1338 (± 1.3)	1341 (± 0.3)	1341 (± 0.3)	1337 (74)	NO_2 stretch	1288 (24)	49 ν(N−O), 30 $\nu(C-N)_{NO}$
1412	1401 (± 0.8)	1402 (± 0.3)	1403 (± 0.4)	1394 (76)	N=N stretch + ring A	1438 (19)	39 ν(C−C), 25 ν(N−O), 17 ν(N=N)
		1427 (± 1.0)	1427 (± 0.6)				
1449	1448 (± 1.2)	1452 (± 0.6)	1452 (± 0.3)	1454 (79)	N=N stretch	1462 (18)	45 ν(N=N), 31 ν(N−O)
1470				1472 (80)	phenyl−N=N stretch + ring deformation		
1492				1498 (82)	phenyl−N=N stretch + ring deformation		
1594	1595 (± 0.7)	1593 (± 0.4)	1595 (± 0.4)	1589 (86)	CC ring stretch	1659 (10)	70 ν(C−C), 19 δ(C−C)

[a] Mean ± standard deviation for six samples, unless noted otherwise. [b] Mode number is in parentheses. [c] Ring A, phenyl group with NO_2 group; ring B, phenyl group without NO_2 group. [d] Adapted from ref 54. [e] ν, stretch; δ, in-plane bend. [f] Mean ± standard deviation for five samples. [g] Mean ± standard deviation for two samples.

similar to that reported previously for NAB chemisorbed to glassy carbon.[36] PPF and GC are structurally similar, with the exception that the PPF surface is much flatter than that of polished GC. So the similarity of NAB spectra on PPF and GC is not surprising. Peak frequencies and assignments for the spectra of Figure 1 are listed in Table 1, based on previous analysis and literature spectra. The improved signal/noise ratio of the line focused spectrometer permitted observation of several previously unreported low-frequency surface Raman bands in the 500−1000-cm^{-1} range, shown in Figure 1 for NAB(4.5). Several of these modes are listed in Table 1 along with tentative assignments. Sample positioning was sufficiently reproducible that peak intensities correlated quantitatively with NAB thickness. Based on the 32% coverage of the submonolayer, its average thickness is 0.5−0.6 nm. Plots of peak intensity versus thickness were linear for all peaks apparent in Figure 1, with the exception of the 1125- and 1271-cm^{-1} bands. Close examination of the spectra from the three NAB thicknesses reveal some differences. The peak assigned to the phenyl−NO_2 stretch is observed at 1106 cm^{-1} in NAB(1.9) and NAB(4.5), but for submonolayer NAB, this band is a shoulder on the 1125-cm^{-1} peak. A relatively small band is observed in the spectrum for submonolayer NAB at 1271 cm^{-1}. Both of these peaks are not detected in the spectra collected from NAB(1.9) and NAB(4.5). A weak feature at ∼1240 cm^{-1} is apparent in all three NAB/PPF spectra and is likely due to a phenyl−phenyl C−C stretch between the PPF and NAB. Another spectral anomaly is the appearance of a peak at 1425 cm^{-1} in the top two spectra, which is not present in the spectrum taken from submonolayer NAB. Raman peaks and their normal mode assignments are summarized in Table 1.

Figure 2 shows Raman spectra of a NAB(4.5)/PPF surface before and after deposition of Ti to an average thickness of 1.0 nm. The top spectrum (Figure 2a) was collected from the half of the sample under a mask during metal deposition. Spectrum b was collected within 1 h of Ti deposition and shows significant changes of intensity for the ∼1107-, ∼1340-, and ∼1450-cm^{-1} bands, which are associated with normal modes involving the NO_2 group. As reported previously, the peaks at 1107 and 1340 cm^{-1} are assigned to the phenyl−NO_2 stretch and the NO_2 symmetric stretch, respectively.[33,36] Based on the Gaussian 98 calculations, the 1450-cm^{-1} peak is assigned to an N=N stretch of the azo

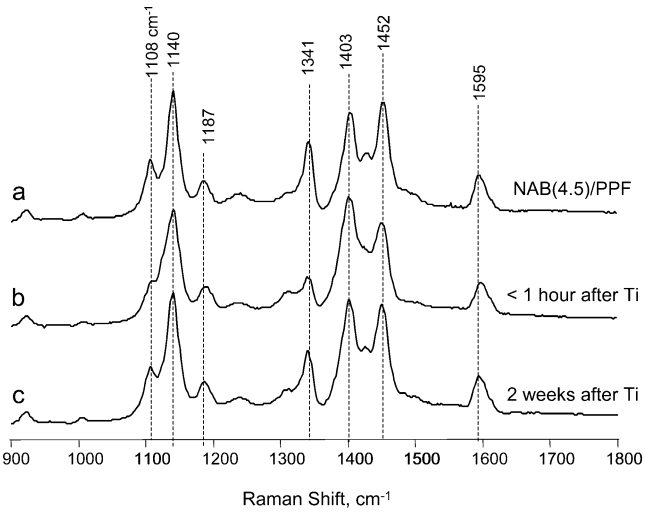

Figure 2. Raman spectra of a NAB(4.5)/PPF surface without (spectrum a) and with (spectra b, c) deposition of 1.0 nm of titanium. Spectra b and c were obtained at the times indicated after Ti deposition with the sample exposed to air. Raman conditions same as those of Figure 1.

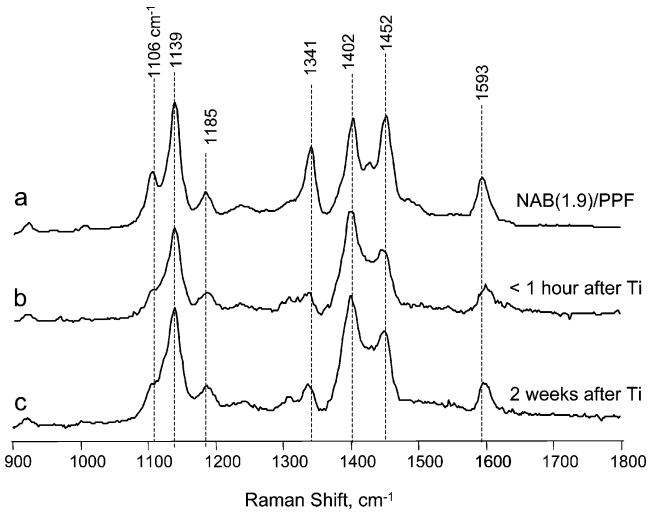

Figure 3. Same as Figure 2, but for a 1.9-nm-thick layer of NAB on PPF.

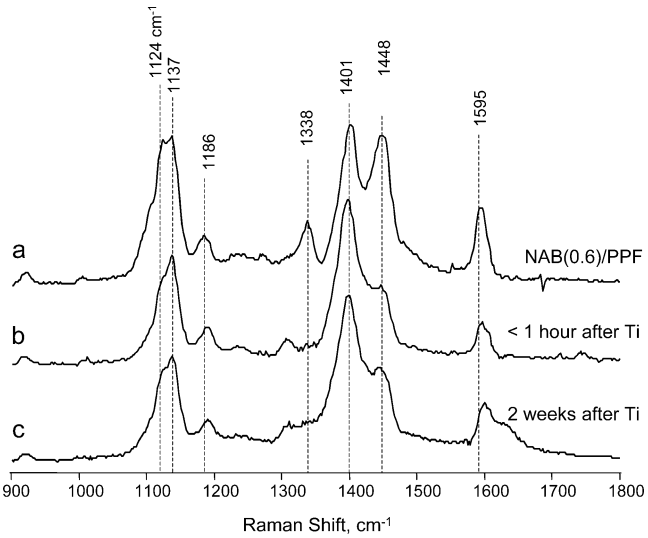

Figure 4. Same as Figure 2, but for a submonolayer of NAB on PPF having an average thickness of 0.6 nm.

group, but Biswas and Umapathy further concluded that this mode is coupled to the NO_2 stretch.[54] The intensity of the bands not associated with the NO_2 group were unaffected by Ti deposition, except for a slight decrease in absolute intensity. Comparison of the 1140-cm^{-1} band intensity on the metallized and unmetallized regions revealed a decrease of 2−13% from Ti deposition on the NAB(4.5) sample. Spectra taken over a period of two weeks after Ti deposition showed a slow increase in the bands associated with the nitro group. The bottom spectrum (Figure 2c) was collected two weeks after the sample was removed from the deposition chamber and kept in air. It shows appreciable increases in the intensities of the ∼1107-, ∼1340-, and ∼1450-cm^{-1} bands, which recover to ∼50% of their intensity before metal deposition. For a separate NAB sample, deposition of a 3.0-nm thickness of Ti resulted in qualitatively similar effects on the Raman spectra. The 1342-cm^{-1} peak intensity decreased upon Ti deposition and then gradually increased to ∼50% of its value before Ti deposition. No differences in the behavior of the 1.0- and 3.0-nm Ti/NAB(4.5)/PPF samples were apparent by Raman spectroscopy. Deposition of an additional 9.0 nm of Au on top of 1.0 nm of Ti without breaking vacuum had no effect on the shape of the Raman spectra, indicating that exposure of Ti to air did not affect the observed behavior.

Analogous spectra of Ti deposited on NAB(1.9)/PPF and NAB(0.6)/PPF are presented in Figures 3 and 4, respectively. Similar changes are apparent as the same peaks associated with the NO_2 group decrease in intensity after Ti deposition. However, these spectra do not show a significant recovery of the NO_2 peaks as was observed for NAB(4.5)/PPF. In fact, the spectrum corresponding to submonolayer NAB exhibits complete loss of the NO_2 stretch at 1340 cm^{-1}, which does not recover during the two-week observation period. If the Ti thickness was increased to 3 nm on submonolayer NAB on PPF, the spectral changes were similar, with the 1340-cm^{-1} band being permanently suppressed.

Figures 5 and 6 show the results of two "control" experiments to confirm the importance of both Ti and the NO_2 group to the observed spectral changes. Figure 5 shows the effect of depositing gold (1.0 nm) rather than Ti on NAB(1.9)/PPF. No change in relative intensity of any of the peaks was detected, even those whose normal modes are associated with the NO_2 group. Figure 6 shows the effect of Ti deposition on an azobenzene monolayer on PPF, prepared and examined in a manner identical to that used for Figures 2−4. The absolute intensity decreases ∼50% upon Ti

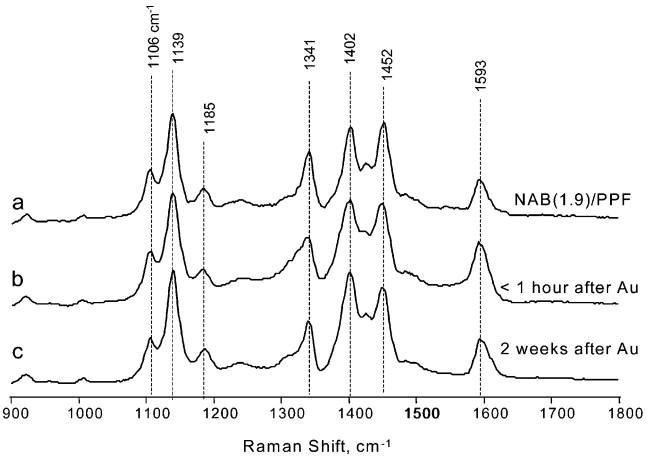

Figure 5. Same as Figure 3, but for Au deposition on NAB(1.9)/PPF.

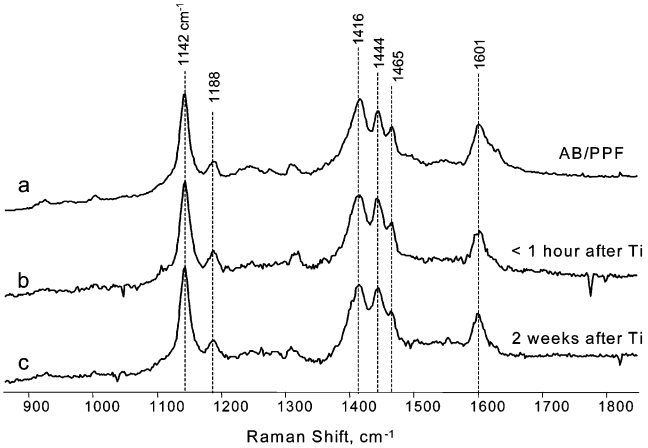

Figure 6. Raman spectra following Ti deposition on an azobenzene monolayer on PPF. Conditions same as those of Figure 2.

(54) Biswas, N.; Umapathy, S. *J. Phys. Chem. A* **2000**, *104*, 2734.

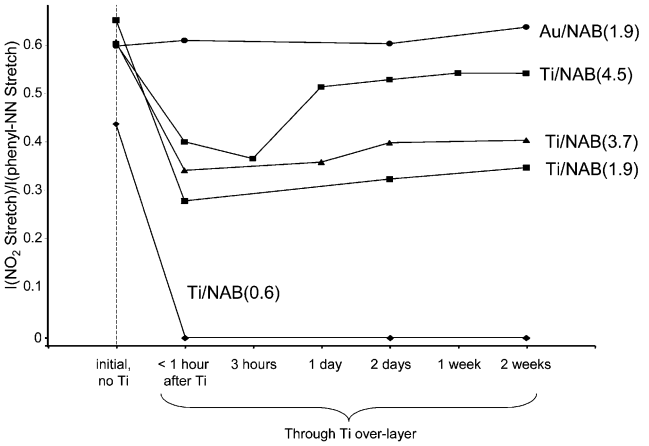

Figure 7. Time course of the 1340-cm^{-1} NO_2 Raman band following deposition of 1.0 nm of Ti or Au, as indicated. Ordinate is the ratio of the 1340-cm^{-1} peak height (relative to a linear baseline) to that of the 1138-cm^{-1} peak height.

deposition, but no changes in relative peak intensities were observed. Furthermore, no new spectral features were observed after Ti deposition on azobenzene, although some very weak peaks were more difficult to observe due to reduced signal (e.g., ~1240 cm^{-1}).

Figure 7 shows how the relative intensity of the NO_2 stretch at ~1340 cm^{-1} changes with time. Relative intensities were used to account for variations in sample focus, instrument alignment, and laser power fluctuations. Absolute intensity was measured from the baseline after applying a linear baseline correction. Intensities were normalized to the peak height of the phenyl−NN stretch at ~1138 cm^{-1}, which is unperturbed by metal deposition. This figure clearly displays the differences in NO_2 recovery for four NAB thicknesses. Immediately following Ti deposition on NAB(4.5), the relative intensity of the ~1340-cm^{-1} peak decreases to 58% of its initial intensity. After two weeks, it increases to 83% of its initial intensity. Similarly, NAB(1.9) exhibits a decrease to 38% of its initial intensity, but after two weeks, the relative intensity of the NO_2 stretch recovers to 54% of it initial intensity. For the case of submonolayer NAB, the peak at ~1341 cm^{-1} is not detected and does not recover after depositing Ti. The relative intensity of the ~1340-cm^{-1} peak of NAB(1.9) is unchanged by the deposition of Au and shows no variation over the entire two-week period. The trend of relative intensity is also shown for an NAB/PPF sample with a thickness of 3.7 nm, equal to that studied previously.[1]

Photoelectron Spectroscopy. Although exposure of samples to air was minimized (<10 min) between NAB or metal deposition and loading in the XPS, it is likely that oxidation of the thin Ti film occurred. Hence, the O_{1s} XPS peak was not analyzed in detail. No observable XPS peak for fluorine (687 eV[55]) appeared in any of the XPS spectra, indicating the absence of detectable fluoroborate residue from the NAB deposition solution. Observed N_{1s}, C_{1s}, and Ti_{2p} XPS binding energies are listed in Table 2 along with literature values for possible surface species. Survey spectra of each sample were used to determine the atom percent of each element, with the results listed in Table 3. As reported previously, unmodified PPF has a low level of surface oxides (<2%), which increases gradually over a period of several days to ~8%.[46] The NAB(1.9)/PPF sample without metal deposited has approximately the expected N/O ratio of 3/2 for NAB, but the C/N ratio is much higher than expected due to signal from the underlying PPF. The N/O ratio on submonolayer NAB is lower than expected, presumably due to oxidation of the PPF during derivatization and handling. As expected, the surface oxygen level on the Ti-treated samples is quite high, due mainly to the formation of TiO_x.

The high-resolution N_{1s} XPS spectra for NAB(1.9)/PPF, Ti/NAB(1.9)/PPF, Ti/NAB(4.5)/PPF, and Au/NAB(1.9)/PPF are shown in Figure 8. The spectrum for NAB(1.9) shows the expected peaks for nitro and azo nitrogen atoms at 406.1 and 400.0 eV, respectively.[33] The expected binding energies for unreacted $R-N_2^+$ are 405.1 [56,57] and 403.8 eV,[56] and their absence in Figure 8a implies negligible presence of unreacted NAB N_2^+ reagent. Deposition of Ti on NAB(1.9)/PPF (Figure 8b) results in complete loss of the 406.1-eV peak and the formation of a new peak at 397.0 eV, which is characteristic of a Ti−N bond.[58−60] When Ti was

Table 2. Observed Binding Energies and Assignments for Ti/NAB/PPF Junctions

	binding energy (eV) observed	assignment	binding energy, lit.	refs
N ls	406.1	nitro	406	33
	400.0	azo	400	33
		$R-N_2^+$	405.1	56, 57
		$R-N_2^+$	403.8	56
		tetrabutyl-ammonium	~401.5	74, 75
	397.0	Ti−N	396.9−397.4	58−60
	401.4	NO	399.7−401.6	70, 76
Ti 2p	459.0	TiO_2 (2p3/2)	459.0−458.7	55, 61−64
	464.7	TiO_2 (2p1/2)	464.4−464.5	55, 61,64
	457.0	Ti_2O_3 (2p3/2)	456.6−457.1	61, 64
	461.5	Ti_2O_3 (2p1/2)	461.8−462.8	61, 64
		TiO (2p3/2)	454.4−455.3	61, 64
		TiO (2p1/2)	460.0−460.9	61, 64
	455.4	Ti−N (2p3/2)	455.2−455.8	58−60, 65
		Ti (2p3/2)	453.9	64, 65
		Ti−C	454.6−454.7	66, 67
C ls	284.5	graphite	284.5	46
	282.2	Ti−C	281.5	65−67

Table 3. Surface Atom Percentages from XPS Survey Spectra

	% N	% C	% O	% Ti	% Au
Ti/NAB(4.5)/PPF[a]	4.3	45.2	30.1	19.7	
Ti/NAB(1.9)/PPF	3.7	47.2	31.1	18.0	
Ti/PPF		46.1	36.3	17.6	
Au/NAB(1.9)/PPF	4.8	69.2	4.6		21.5
Au/PPF		80.3	2.0		17.6
NAB(1.9)/PPF	7.1	87.0	5.9		
NAB(0.6)/PPF	2.5	93.4	4.1		
PPF		98.8	1.2		
NAB(calculated)	12.0	48.0	8.0		

[a] Ti and Au thicknesses were 1.0 nm in all cases, determined as average thickness with a quartz microbalance.

(55) Moulder, J. F.; Stickle, W. F.; Sobol, W. F.; Bomben, K. D. *Handbook of X-ray Photoelectron Spectroscopy*; Perkin-Elmer Corp., Physical Electronics Div.: Eden Prairie, MN, 1992.

(56) Finn, P.; Jolly, W. L. *Inorg. Chem.* **1972**, *11*, 1434.

(57) Brant, P.; Feltham, R. D. *J. Organomet. Chem.* **1976**, *120*, C53.

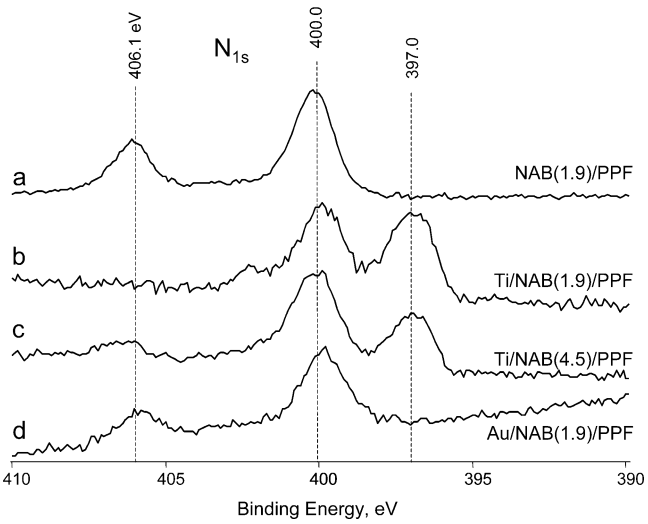

Figure 8. XPS spectra of N_{1s} region of NAB/PPF samples, with NAB thickness as indicated. Ti thickness was 1.0 nm.

Table 4. Surface Atom Percentages for Nitrogen, from High-Resolution XPS

	% N (406)	% N (400)	% N (397)	sum	from survey
Ti/NAB(4.5)/PPF	0.55	3.6	1.0	5.2	4.3
Ti/NAB(1.9)PPF		2.0	1.6	3.6	3.7
Au/NAB(1.9)/PPF	1.9	3.8		5.7	4.8
NAB(1.9)/PPF	2.8	5.0		7.8	7.1
NAB(0.6)/PPF	1.0	2.0		3.0	2.5
NAB(calculated)	4.0	8.0	0	12	12

deposited on a 4.5-nm NAB film, (Figure 8c), a Ti−N bond is also formed, but the nitro group is not completely lost. Integrated peaks areas reveal that 8% of the total nitrogen remains in the form of NO_2 and ∼30% of the nitrogen atoms are now bound to the titanium in the Ti/NAB(4.5)/PPF sample. The spectrum for Au/NAB(1.9)/PPF (Figure 8d) shows no sign of Au−N bond formation, based on the preservation of the position and shape of the nitro and azo peaks and the absence of additional peaks. The distribution of surface nitrogen among the 406 (nitro), 400 (azo or nitroso), and 397 (Ti−N) species obtained from high-resolution N_{ls} XPS spectra are listed in Table 4.

The Ti 2p XPS spectra for Ti/NAB(1.9), Ti/NAB(4.5), and Ti deposited directly on PPF (Ti/PPF) are shown in Figure 9. The absence of a Ti° peak at 454.0 eV implies nearly total reaction of the thin Ti layer with the sample or atmospheric oxygen. All three spectra show prominent peaks at 464.7 and 459.0 eV, which are assigned to the Ti $2p^{1/2}$ and Ti $2p^{3/2}$ peaks of TiO_2, respectively.[55,61−64] Deconvolution indicates that Ti is also present

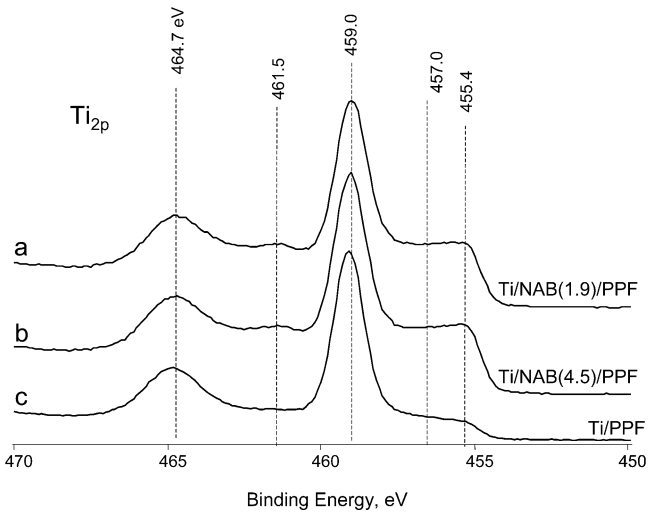

Figure 9. XPS spectra for Ti_{2p} region following deposition of 1.0 nm of Ti on NAB(1.9)/PPF (a), NAB(4.5)/PPF (b), and on unmodified PPF (c).

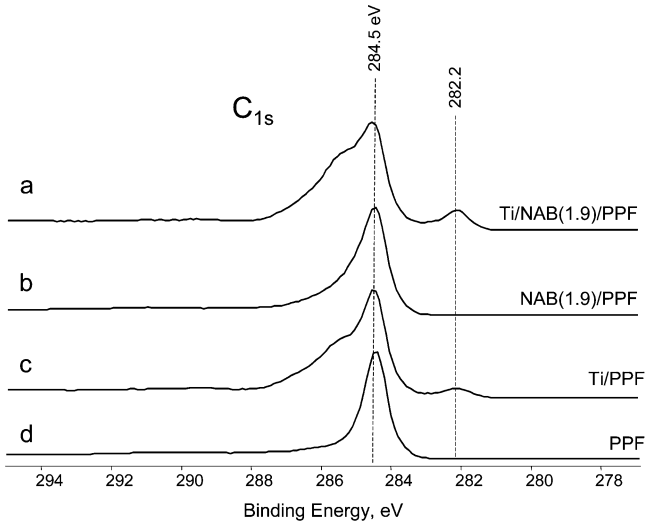

Figure 10. XPS spectra of C_{ls} region with and without a 1.0-nm layer of Ti, as indicated.

as Ti_2O_3, with peaks at 461.5 and 457.0 eV.[61] The Ti/NAB(1.9) and Ti/NAB(4.5) spectra show a low-binding energy peak at 455.4 eV, which can be attributed to the Ti $2p^{3/2}$ band of either Ti−N or Ti−C. Since a literature search revealed the Ti−C peak to occur at a binding energy ∼1 eV lower than 455.4 eV, Ti−N is the more likely assignment.[58−60,65,66] The spectrum for Ti/PPF also shows a weak shoulder at 455.4 eV, with an area of 2% of the total Ti 2p signal. This ∼455-eV feature on Ti/PPF is much weaker than that when NAB was present and could be due to Ti−C or TiO($2p^{3/2}$).

The C_{1s} XPS spectra for Ti/NAB and Au/NAB are shown in Figure 10. All spectra include the C_{1s} peak for graphitic carbon at 284.5 eV, which has been reported previously for PPF surfaces.[46] After depositing Ti, a low-binding energy peak is detected at 282.2 eV for Ti/NAB(1.9), Ti/NAB(4.5), and Ti/PPF (Figure 10a−c, respectively). This feature is commonly observed in metal

(58) Biwer, B. M.; Bernasek, S. L. *Surf. Sci.* **1986**, *167*, 207.
(59) Shulg'a, Y. M.; Troitskii, V. N.; Aivazov, M. I.; Borodk'o, Y. G. *Zh. Neorg. Khim.* **1976**, *21*, 2621.
(60) Badrinarayanan, S.; Sinha, S.; Mandale, A. B. *J. Electron Spectrosc. Relat. Phenom.* **1989**, *49*, 303.
(61) Gonbeau, D.; Guimon, C.; Pfister-Guillouzo, G.; Levasseur, A.; Meunier, G.; Dormoy, R. *Surf. Sci.* **1991**, *254*, 81.
(62) Slinkard, W. E.; DeGroot, P. B. *J. Catal.* **1981**, *68*, 423.
(63) Murata, M.; Wakino, K.; Ikeda, S. *J. Electron Spectrosc. Relat. Phenom.* **1975**, *6*, 459.
(64) Saied, S. O.; Sullivan, J. L.; Choudhury, T.; Pearce, C. G. *Vacuum* **1988**, *38*, 917.
(65) *Practical Surface Analysis, Vol. 1: Auger and X-ray Photoelectron Spectroscopy*; 2nd ed.; Briggs, D., Seah, M. P., Eds.; John Wiley and Sons: Chichester, 1990.
(66) MacInnes, A. N.; Barron, A. R.; Li, J. J.; Gilbert, T. R. *Polyhedron* **1994**, *13*, 1315.

carbides[65−67] and indicates the formation of a Ti−C bond. The area of the 282.2-eV peak following Ti depostion was 7% of the total C_{1s} signal for NAB(1.9), 8% for NAB(4.5), 5% for bare PPF, and 6% for azobenzene on PPF. The high-binding energy shoulder on the 284.5-eV graphitic carbon peak was observed whenever Ti was present and is likely due to adventitious carbon adsorbed to the Ti.

Deposition of Au on NAB-modified PPF and unmodified PPF does not result in a change in the C_{1s} peak position or line shape, and no new peaks were detected. These observations indicate that there is no observable chemical reaction between the NAB film and the Au overlayer. The O_{1s} XPS peak for all samples with a Ti overlayer appeared at 530.6 eV (data not shown), which is characteristic of an oxygen atom in TiO_2.[61,62] Depositing Au on the NAB(1.9)/PPF sample did not shift the position of the O_{1s} peak at 532.7 eV. The Au $4f_{7/2}$ and $4f_{5/2}$ peaks were observed at 84.0 and 87.7 eV, respectively, when Au was present, as expected from the binding energies of metallic Au (84 and 88 eV).[55]

DISCUSSION

The Raman spectrum of an NAB monolayer in the 900−1700-cm^{-1} range on glassy carbon was discussed previously in detail,[33,36] but additional insights are available from the current results on PPF. The similarity of the submonolayer spectrum (Figure 1a) on PPF to an NAB monolayer on GC implies similar bonding between the NAB and the disordered sp^2 carbon surfaces. The weak feature at 1240 cm^{-1} is likely to be from the C−C bond between the ring B (the phenyl ring without the NO_2 group) in NAB and the carbon surface. Spectra of NAB on both GC and PPF are significantly different from that of NAB in solution, implying a strong interaction between NAB and the covalently bonded sp^2 carbon solid. Previous results from NAB bonded to the edge plane of ordered graphite indicated an increase in Raman cross section of 2−3 orders of magnitude compared to that in solution, reinforcing the presence of a strong NAB/PPF interaction.[33] Furthermore, the bands most strongly perturbed by NAB chemisorption (1470 and 1492 cm^{-1}) are associated with the N═N group, implying coupling of this bond to the graphite surface. While there are various possibilities for the origin of these effects of NAB chemisorption, a likely source is changes in resonance Raman enhancement caused by electronic coupling between the NAB and the conducting sp^2 carbon matrix.

The submonolayer of NAB, with an average thickness of 0.6 nm and a coverage of 32%, was examined initially in order to avoid contributions from multilayers. As noted earlier, the NAB(0.6) spectra are identical to those reported previously for a full monolayer. It should be emphasized that the NAB(0.6) sample resulted from spontaneous chemisorption of NAB without an applied potential, presumably via electron transfer from the bulk PPF film to the NAB N_2^+ reagent. The NAB(1.9) sample corresponds to slightly more than a monolayer, since the calculated length of an NAB molecule oriented normal to the PPF surface is 1.45 nm. Both the NAB(1.9)/PPF and NAB(4.5)/PPF spectra exhibit a 1425-cm^{-1} Raman peak and the absence of the 1125-cm^{-1} peak. While these features are currently unassigned, we attribute them to bonding between NAB molecules in a multilayer. The 1240-cm^{-1} phenyl−phenyl stretch is expected both for NAB−PPF and NAB−NAB; hence, its intensity relative to nearby bands does not vary with thickness. The fact that the Raman intensity tracks the NAB thickness linearly implies that both the NAB submonolayer and NAB multilayer films have comparable Raman cross sections, indicating a similar degree of enhancement regardless of thickness. Consistent with the observations of Kariuki and McDermott,[32] multilayer formation appears to proceed by addition of a second or third NAB radical, resulting in an extended, resonance-enhanced, multilayer.

Slow deposition (0.03 nm/s) of a thin layer of Ti (1.0 nm) did not affect the NAB spectrum greatly, except for the modes associated with the NO_2 group. The absence of major changes in the NAB Raman spectrum upon Ti deposition indicates that the NAB layer is largely intact, both soon after Ti deposition and two weeks later. The phenyl−NO_2 stretch (∼1107 cm^{-1}), the NO_2 stretch (∼1340 cm^{-1}), and the N═N stretch coupled to NO_2 (∼1450 cm^{-1}) all lose intensity upon Ti deposition. These changes are qualitatively similar to those observed with in situ Raman spectroscopy during the electrochemical reduction of NAB chemisorbed to glassy carbon.[36] In that case, the NO_2 and N═N intensities decreased upon reduction, and the 1100−1130-cm^{-1} region changed peak shape. For the case of the NAB submonolayer in the current report, the NO_2 stretch is completely and permanently suppressed by Ti deposition. As shown in Figure 7, the NO_2 stretch partially recovers for NAB layers from 1.9 to 4.5 nm thick over a period of several days. The XPS results demonstrate a reaction of the Ti with the NO_2 group to form a Ti−N bond, with complete removal of the N_{1s} peak for NO_2 (406.1 eV) in the NAB(0.6) and NAB(1.9) samples In a UHV study, Campion et al. concluded that nitrobenzene chemisorbed spontaneously to nickel to produce nitrosobenzene and adsorbed oxygen.[68,69] A decrease in intensity of all Raman peaks associated with the nitro group was observed and a new peak assigned to the nitroso N═O stretch appeared. Kishi and co-workers used XPS to characterize nitrobenzene chemisorption on nickel and iron surfaces.[70] On an evaporated metal surface, nitrobenzene dissociates in steps, producing adsorbed nitrosobenzene, and then a nitrogen anion after releasing the two oxygen atoms to form surface oxides. In the present case of Ti on NAB, the fact that the spectrum following 3.0 nm of Ti behaves very similarly to that after 1.0 nm of Ti implies that the first Ti layer has modified the NAB layer and that additional Ti deposition has no observable effect. Furthermore, protection of the Ti with a Au layer had no effect on the spectra, implying that air oxidation of the Ti is unimportant to the Raman results and that a Ti/air interaction is not responsible for the recovery of the NO_2 Raman features observed for NAB(4.5). Preliminary calculations of model Ti−nitrosophenyl structures with Gaussian 98 indicate a three-center bond between Ti, N, and O, with a Ti−N bond length of 0.20 nm and a Ti−O bond length of 0.19 nm.

The formation of a Ti−N bond is important in the context of molecular electronics, since it demonstrates a covalent contact between the Ti and NAB. There is a high probability that the Ti bonded to the NAB is in electrical contact with bulk Ti metal for a thick (>3.0 nm) Ti layer, possibly with an oxygen atom bonded to the Ti. The phenyl−NO−Ti linkage between NAB and Ti,

(67) Galuska, A. A.; Uht, J. C.; Marquez, N. *J. Vac. Sci. Technol. A* **1988**, *6*, 110.
(68) Campion, A.; Brown, J. K.; Grizzle, V. M. *Surf. Sci. Lett.* **1982**, *115*.
(69) Campion, A. *Annu. Rev. Phys. Chem.* **1985**, *36*, 549.
(70) Kishi, K.; Chinomi, K.; Inoue, Y.; Ikeda, S. *J. Catal.* **1979**, *60*, 228.

combined with the C−C bond between NAB and PPF, makes the resulting molecular junction covalent at both contacts. Lindsay et al., have demonstrated that a covalent contact between Au and organic monolayers reduced the contact resistance by 3 orders of magnitude compared to a noncovalent contact with a conducting scanning probe microscopy tip.[71−73] The lower energy barrier of a covalent contact is likely to be very important for practical realization of electronic devices based on molecular junctions.

The recovery of the NO_2 stretch at ∼1340 cm^{-1} for the 1.9- and 4.5-nm layers (Figure 7) implies temporary reduction of the nitro group by the deposited Ti. Ti is a strong reducing agent, and the high free energy of Ti atoms is likely to increase their tendency to reduce whatever is available. Upon deposition of Ti, electrons are apparently injected into the NAB layer, sufficient to reduce most of the NO_2 groups present. The nitro groups on the NAB layer surface irreversibly form Ti−N bonds but NO_2 groups deeper in the film apparently do not. The recovery of the ∼1340-cm^{-1} Raman feature with time is due to slow reoxidation of "deep" NO_2 groups, presumably by air in contact with the Ti or PPF.

We have reported separately on molecular junctions with 3.7-nm NAB layers between PPF and Ti, which are very similar to those studied here, except that the Ti layer was 40 nm thick and was protected from air by a 100-nm layer of gold. We concluded that electron injection into the film caused either by Ti deposition or an imposed electric field caused a dramatic increase in junction conductivity.[1] Furthermore, the junctions had high conductivity for several hours after Ti deposition, which decreased over a period of several days. The increase of junction resistance correlates with the recovery of the ∼1340-cm^{-1} Raman feature reported here (Figure 7), consistent with the conclusion that electron injection and NO_2 reduction are responsible for the observed conductivity change.

The absence of any observable changes in the Raman and XPS spectra of NAB upon deposition of gold is consistent with the low reactivity of Au, particularly as a reducing agent. In addition, gold deposition should cause local heating during condensation which is approximately equal to that of Ti, so the spectral changes accompanying Ti deposition are not likely to result merely from heat. The appearance of a weak Ti−C XPS peak at 282.2 eV (Figure 10) for Ti deposition on NAB indicates that some Ti penetrated the NAB layer and reacted with either PPF or the phenyl rings of NAB. However, the carbide band was 8% of the total carbon or less, and the NAB Raman intensity attenuation (4−13%) was approximately the magnitude expected from absorption losses in the Ti film. These observations imply that the nitro group of NAB provides a means to anchor the initial layer of reactive Ti atoms on the NAB surface, in the form of Ti−NO− phenyl linkages. Subsequent Ti atoms then form additional Ti layers on top of the "anchored" Ti monolayer, until bulk, conducting Ti metal is formed. Some Ti penetrates the NAB layer to form Ti−C and presumably Ti−azo bonds, possibly at defect sites. For Ti on azobenzene, the absence of nitro groups may permit increased reaction between Ti and the organic layer, leading to a larger decrease in Raman intensity. However, the ability to make Au/Ti/NAB(3.7)/PPF molecular junctions with a low incidence of short circuits indicates that the Ti that penetrates the NAB does not form a path for metallic conduction.[1] The dynamic behavior of such junctions as molecular electronic components is strong evidence against the contribution of metal or metal carbide defects to the electronic properties of Au/Ti/NAB(3.7)/PPF junctions.

In summary, the Raman and XPS results permit several conclusions about the structure of Ti/NAB/PPF molecular junctions. First, the NAB multilayer (1.9−4.5 nm) is structurally similar to a monolayer, at least as indicated in the Raman spectra for different thicknesses. Multilayer formation presumably occurs via attack of electrogenerated NAB radicals on the first NAB monolayer, as observed by Kariuki and McDermott for a different diazonium reagent.[32] Second, vapor-deposited Ti atoms react with the NO_2 groups on the surface of the NAB layer to form a Ti−N bond, probably a Ti−nitroso covalent linkage. Third, Ti deposition temporarily reduces the NO_2 groups that have not bonded to Ti, presumably to form the NAB anion radical or quinoid species. These reduced NO_2 groups recover over an approximately one-day period, presumably through reoxidation by air. Fourth, the reaction between Ti and NO_2 appears to decrease the incursion of Ti atoms into the NAB layer, thus reducing the possibility of forming short circuits. This behavior is similar to that reported by Allara et al., for metal deposition on Au/thiol SAMS, for which a carboxylate terminal group prevented Ag penetration into the SAM.[29,30] Finally, we plan to report spectroscopic monitoring of active molecular junctions using similar Raman techniques in a separate publication.

(71) Cui, X. D.; Primak, A.; Zarate, X.; Tomfohr, J.; Sankey, O. F.; Moore, A. L.; Moore, T. A.; Gust, D.; Harris, G.; Lindsay, S. M. *Science* **2001**, *294*, 571.

(72) Cui, X. D.; Primak, A.; Zarate, X.; Tomfohr, J.; Sankey, O. F.; Moore, A. L.; Moore, T. A.; Gust, D.; Nagahara, L. A.; Lindsay, S. M. *J. Phys. Chem. B* **2002**, *106*, 8604.

(73) Rawlett, A. M.; Hopson, T. J.; Nagahara, L. A.; Tsui, R. K.; Ramachandran, G. K.; Lindsay, S. M. *Appl. Phys. Lett.* **2002**, *81*, 3043.

(74) Elliott, C. M.; Murray, R. W. *Anal. Chem.* **1976**, *48*, 1247.

(75) Saby, C.; Ortiz, B.; Champagne, G. Y.; Belanger, D. *Langmuir* **1997**, *13*, 6805.

(76) Batich, C. D.; Donald, D. S. *J. Am. Chem. Soc.* **1984**, *106*, 2758.

ACKNOWLEDGMENT

This work was supported by the National Science Foundation through project 0211693 from the Analytical and Surface Chemistry Division.

Received for review July 16, 2003. Accepted December 1, 2003.

AC034807W